Kinetics of Monolayer Bi Electrodeposition on Au(111): Surface X-ray Scattering and Current Transients

K. Tamura,[†] J. X. Wang,[‡] R. R. Adžic,[‡] and B. M. Ocko*,[†]

Department of Physics and Materials Science Department, Brookhaven National Laboratory, Upton, New York 11973-5000

Received: September 23, 2003; In Final Form: December 4, 2003

The kinetics of Bi monolayer electrodeposition (underpotential deposition) on the Au(111) electrode was investigated using surface X-ray scattering and electrochemical methods. The current and X-ray intensity transients were measured simultaneously using a low-resistance drop cell that has a potential response time less than 50 μs. Three independent measurements of the Bi coverage transients were obtained, which are related to (1) the integrated charge, (2) the adsorbed Bi, irrespective of the adsorption site, and (3) the adsorbed Bi with a well-defined (2×2) structure. The zero-coverage ↔ commensurate (2×2)-Bi phase transition occurs on the millisecond time scale, 3 orders of magnitude more rapidly than the (2×2)-Bi ↔ high-coverage incommensurate $(p\times\sqrt{3})$-2Bi phase transition. Nucleation and growth kinetics was observed for both transitions involving Bi desorption. Langmuir adsorption kinetics was observed for both transitions involving Bi adsorption. Comparison of the total coverage with that measured by in-plane diffraction intensity suggests fast coarsening of islands for the transition for the zero-coverage ↔ commensurate (2×2)-Bi phase transition.

1. Introduction

During the past decade, our atomic level understanding of electrode surfaces has greatly expanded due to the development of in situ scanning probe and surface X-ray scattering techniques. It is now possible to directly investigate the structure of electrode surfaces versus the applied potential under a variety of chemical conditions and to directly correlate the features observed in electrochemical measurements with specific structural changes.[1] Despite these advances, much less is known about the structure of electrode surfaces under high current conditions due to the difficulty in reducing potential drop over the sampling area in a thin-layer cell or under the STM tip.

Potential step methods have been used to investigate a variety of metal deposition phenomena and have helped in providing a thermodynamic description of their kinetics.[2] A well-defined current peak following the potential step at a characteristic time is suggestive of nucleation and growth kinetics, either progressive or instantaneous.[3] Likewise, exponential transients typically imply Langmuir adsorption where the probability of adsorption depends on the number of available sites[4,5] and not on the circumference of the growing islands. Structural details on the nature of the growth after adsorption process, such as the domain distribution, cannot be ascertained from these current measurements alone.

A longstanding goal of researchers in the electrochemical kinetics growth community has been to develop a structural basis for the proposed transient growth models. Scanning probe microscopy and X-ray scattering (SXS) are the techniques of choice for achieving this goal; however, geometrical constraints provide practical limitations on the time resolution. With STM transient measurements, the time resolution is limited by the scan rate of the STM tip and the area under investigation. Furthermore, the geometry of the tip can affect the potential distribution and deposition below the tip can be impaired. Despite this, changes in the structure can be observed on time scales as fast as 0.01 s when the scanned region is limited.[6] STM has been used to probe the transient kinetics of surface reconstruction in a Au single crystal,[7−10] the electrodeposition of Pd on Au single crystal,[11] and the desorption of self-assembled monolayer.[12]

Surface X-ray scattering (SXS), which is sensitive to the average structure over the macroscopic region illuminated by the beam, has the potential to measure detailed structural information during electrochemical processes. This technique has been employed to measure the Ag(100). Here a macroscopic area, typically in a few mm^2 is probed. In these measurements, and for those of the formation of the reconstructed Au(111) surface,[16] changes in the diffraction profiles could be observed on the 1 s time scale, thus providing direct information on the slow process if island coarsening.

Conventional *thin-layer* electrochemical cells employed in SXS measurements[16,17] consist of a thin-layer electrolyte, which has a high solution resistance, i.e., high RC constant; thus they are not ideal for fast kinetics measurements. Recently, we have developed an electrochemical cell (a "*drop* cell") that provides a much faster response to a step change of potential than a thin layer cell. This is achieved through the minimization of the solution resistance by placing the counter and reference electrodes very close to the working electrode.[18] The essential feature of the cell, as the name implies, is an electrolyte drop constrained by the working electrode as a base, and the counter and reference electrodes above it, all within 2−3 mm of each other. The potential response time of the cell using 1 M electrolyte is less than 50 μs. The drop is slightly smaller than the 1 cm capillary length of water (the maximum stable drop size), and the cell can be held nearly vertically during X-ray measurements. With a high energy X-ray beam, we demonstrate here that for the first time the in-plane X-ray diffraction intensity transients can be used to follow the structural phase transitions on a millisecond time scale.

[†] Department of Physics.
[‡] Materials Science Department.

10.1021/jp0368435 CCC: $27.50
Published on Web 01/16/2004

The unusual electrocatalytic behavior of Bi thin films has fascinated researchers since the 1970s and these systems have been intensively investigated using electrochemical[19−21] and optical methods.[22] Since the advent of SXS and STM, and AFM, in the early 1990s, detailed structural aspects of Bi UPD along with the related the catalytic activity have been the subject of investigation by the Illinois and Brookhaven groups.[23−27] In previous studies, two ordered Bi monolayer phases were identified using SXS and AFM:[23,24] the commensurate (2×2)-Bi phase with a quarter monolayer coverage and the close-packed (p×√3)-2Bi phase with the coverage varying with potential between 0.61 and 0.67 monolayer. More recently, we have explored the surface structure during the course of electrocatalytic O_2 reduction using SXS with a drop cell.[18]

In the present study, we focus on the kinetics of the structural phase transitions of Bi monolayers. Current and the scattered X-rays transients were measured, the latter at two different reciprocal lattice positions using identical configurations. We show that it is possible to convert the X-ray intensity transients into an effective atomic coverage, thus providing a direct comparison with the coverage obtained from charge transient measurements. Whereas at one of the X-ray positions the signal is sensitive to the total Bi coverage, the other intensity is sensitive to the domain distribution of the ordered phase. A comparison of the two measurements provides information on the lateral diffusion and the growth mechanism of the ordered phases. For the transitions from the low-coverage phase to the ordered (2×2) phase we find that the adsorption follows the exponential behavior expected from random, Langmuir adsorption, followed by the rapid lateral diffusion to form ordered domains. The opposite process, a desorption of the (2×2) phase, proceeds through the nucleation and growth of holes. These holes do not coalesce/coarsen during the desorption process. For the second transitions, between the (2×2)-Bi and (p×√3)-2Bi phase, reliable X-ray data were only possible at one reciprocal space position. With this limited data set, the functional form of the effective coverage suggests a Langmuir growth process for the formation of the (p×√3)-2Bi phase and a nucleation and growth process for the reverse transition.

2. Experimental Section

The Au(111) single crystal, 10 mm in diameter and 3 mm thick, oriented to better than 0.1°, was mechanically polished with 1 μm alumina powder and subsequently electropolished. The final crystal surface was prepared prior to each electrochemical or SXS measurement by flame annealing for several minutes. After cooling in an air atmosphere, the crystal was protected by a drop of electrolyte and transferred to the electrochemical cell. Ag/AgCl (3 M NaCl) was used as the reference electrode, and a Au wire was used as the counter electrode. Solutions were prepared from reagent grade Bi_2O_3 (Aldrich), ultrapure $HClO_4$, and purified water (Millipore).

In the SXS measurements a drop cell (Figure 1) was used. It consists of an electrolyte drop (ϕ = 7−8 mm) and two other electrodes, which are positioned about 2−3 mm above the working electrode. Further details are given in ref 18. To deoxygenate content in the electrolyte, the crystal and electrolyte drop were surrounded by an environment of flowing N_2 gas, which was saturated with water. The latter minimizes the evaporation of the drop during the course of the X-ray experiment.

The SXS measurements were carried out at the National Synchrotron Light Source at beamline ×22A using a four-circle diffractometer in a vertical scattering geometry. The monochromatic beam, λ = 0.386 Å (32 keV), was focused to a 0.4 mm by 0.4 mm spot at the sample using a bent Si(333) monochromator. At 32 keV energy, the 34 mm X-ray attenuation length of water is about 5 times longer than the drop size; therefore, the drop only attenuates the beam by about 20%. A hexagonal coordinate system in which $Q = (a^*,b^*,c^*)\cdot(H,K,L)$, where $a^* = b^* = 4\pi/\sqrt{3}a = 2.25$ Å^{-1}, $c^* = 2\pi/\sqrt{6}a = 0.89$ Å^{-1}, and a = 2.884 Å was used. The scattered X-rays were collimated using 0.055° (fwhm) Soller slits and the intensity was measured with a NaI detector.

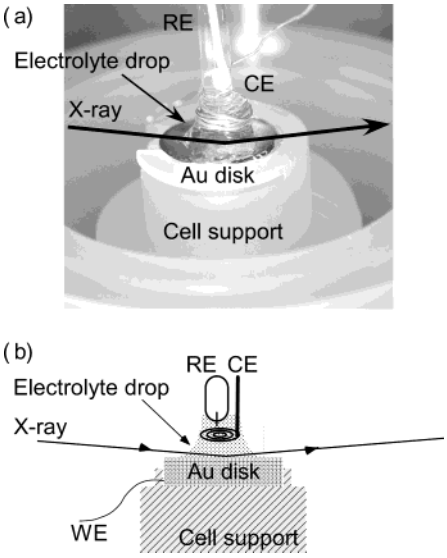

Figure 1. (a) Photographic and (b) schematic cross sectional view of a drop cell for X-ray diffraction/electrochemical measurements.

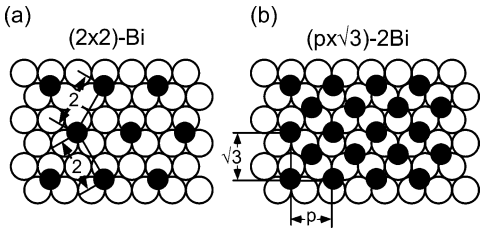

Figure 2. Real space models for the (2×2)-Bi (a) and (p×√3)-2Bi (b) adlayers on Au(111).

The temporal dependent scattering intensity was measured during the course of a periodic potential cycle by summing the signal from at least several thousand cycles. The data were collected using a standard multichannel scaler (MCS) whereby the signal from the different cycles (several thousand cycles) is automatically binned. The current transients utilized the same MCS setup, except for the addition of a current to frequency converter prior to the MCS. Measurements were carried out for the zero-coverage ↔ (2×2) and (2×2) ↔ (p×√3) phase transition and the frequency of the potential step was respectively 10 or 0.02 Hz. The measured potential response of the cell was less than 0.05 ms for the potential pulses used in this study.

3. Results and Discussions

3.1. Cyclic Voltammetry and Potential Dependence of Bi Structure. The atomic structures of the two ordered Bi monolayers determined by previous SXS and STM measurements are illustrated in Figure 2. In the commensurate (2×2) phase, the Bi coverage is 0.25 monolayer with respect to the atomic density of the Au(111) surface. The close-packed

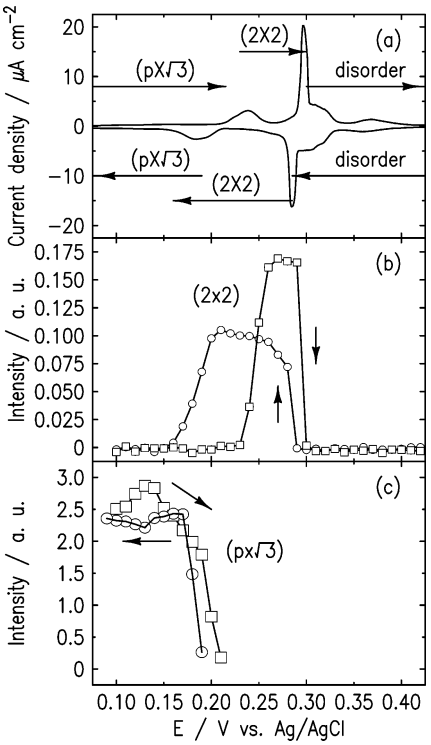

Figure 3. Voltammetry curve (a), diffractogram observed at the ($^1/_2$, $^1/_2$, 0.2) position (b), and integrated intensity for the diffraction peak at the ($-^1/_2+\delta$, $^1/_2+\delta$, 0.2) position (c) for the UPD of Bi on a Au(111) electrode in 1 M $HClO_4$ with 5 mM Bi^{3+}. Sweep rate 2 mV/s for (a) and (b).

($p\times\sqrt{3}$)-2Bi phase can be uniaxially compressed by decreasing the potential, with the Bi coverage increasing from 0.61 to 0.67 monolayer.[18,24] At potentials more positive of the UPD current peaks, the specular reflectivity suggests no adsorbed Bi, thus we refer to this potential region as the zero-coverage phase.

Our kinetic measurements were carried out in 1 M $HClO_4$ solution containing 5 mM Bi^{3+}. A typical voltammetry curve obtained in such a solution at 2 mV/s sweep rate is shown in Figure 3a. With the same sweep rate, the formation and loss of the (2×2) phase were monitored by measuring the X-ray diffraction intensity at the ($^1/_2$, $^1/_2$, 0.2) position. For the incommensurate ($p\times\sqrt{3}$)-2Bi phase, the X-ray intensity near the in-plane diffraction peak is integrated and shown in Figure 3c as a function of potential.

At potentials around 0.28 V, the sharp cathodic and anodic current peaks are accompanied by a big jump and a sudden drop of the (2×2) diffraction intensity, respectively. These data show that fast phase transitions occur near 0.28 V, which involve the formation and loss of the (2×2)-Bi monolayer by Bi electrodeposition and electrodesorption, respectively. The kinetic measurements for these transitions were thus carried out by repetitive potential steps between 0.23 and 0.33 V, given an equal and small overpotential for both phase transitions.

At more negative potentials, the drop of the (2×2) diffraction intensity coincides with the rise of the ($p\times\sqrt{3}$)-2Bi diffraction intensity in a negative potential sweep. This indicates that the disappearance of the (2×2) phase is caused by the additional Bi deposition resulting in the formation of a more densely packed phase. The major change occurs over the potential region where the voltammetry curve shows a broad cathodic current peak. In the positive potential sweep, the ($p\times\sqrt{3}$)-2Bi phase vanishes at slightly more positive potential than the onset of its formation in the negative potential sweep. Yet, it is still slightly more negative than the onset of the (2×2) phase formation and the corresponding cathodic current peak at 0.27 V. Apparently, the phase transitions between these two ordered phases have more hysteresis than the phase transitions between the zero-coverage $\leftrightarrow$ (2×2) phases. Nevertheless, the same potential gap of 0.01 V can be used because the diffraction intensities corresponding to the ($p\times\sqrt{3}$) and (2×2) phases have reached the saturated values at 0.17 and 0.27 V, respectively. The average value of these two potentials, 0.22 V, also corresponds well with the average potential for the cathodic and anodic current peaks. Thus, this pair of phase transitions was also studied by using an equal and small overpotential for both directions.

3.2. Potential Step Experiments. The kinetics of the zero-coverage $\leftrightarrow$ (2×2) and the (2×2)-Bi $\leftrightarrow$ ($p\times\sqrt{3}$)-2Bi phase transitions were studied by simultaneously measuring the current and X-ray scattering intensity after a step change in the potential. To achieve improved time resolution, an electrochemical drop cell was used to reduce the solution phase electrical resistance compared to the conventional thin layer configuration. The longer X-ray path length compared to the thin layer cell was compensated for by the use of higher energy X-rays (32 keV), which reduced the X-ray absorption to about 20% of the incident signal.

The data presented below demonstrates that the transients associated with electrochemical structural phase transitions can be resolved on millisecond time scales. In the X-ray measurements, the weak signal requires continuous pulsing between two potentials so that the signal from multiple pulses could be averaged. This rapid pulsing eventually modifies the surface topography from that of a smooth surface and changes the characteristics of the voltammograms. In the case of a Pt counter electrode, used in preliminary measurements, we found Pt deposits on the Au(111) surface, in the vicinity of the counter electrode, which appeared to grow with the number of potential pulses. Because the potential of the counter electrode is not regulated, it undergoes a high potential transient during every cycle, thus dissolving platinum, which eventually electroplates on the Au(111) surface. Subsequent measurements were carried out with a gold counter electrode, which also dissolves and electroplates onto the Au(111) surface. In this case, the surface roughens with potential pulses cycles but remains as gold. Repetitive potential cycling is well-known to change the topology of surfaces. In the study of Cu UPD on Au(111) and Ag UPD on Pt(111), Mishima and co-workers have found that repetitive pulsing leads to the formation of terraces, oriented perpendicular to the initial steps. Thus, the fast pulsing limited the useful lifetime of the crystal surface to about 10 000 potential cycles.

3.2.1. (2 × 2)-Bi → Zero-Coverage Phase Transition. Current and X-ray intensity transients for the phase transitions between the (2×2) and the zero-coverage phases were measured by stepping the potential between 0.23 and 0.33 V with a duration of 36 ms at each potential. Figure 4 shows the results for the positive potential step, corresponding to electrodesorption of the (2×2)-Bi phase. At the (0, 0, 0.4) position, the in-plane wave vector is zero and thus the X-ray intensity is related to the change of the Bi coverage regardless of their lateral positions. In contrast, the intensity transient measured at the ($^1/_2$, $^1/_2$, 0.2) in-plane position is sensitive only to the (2×2) ordered domains. Thus, the former provides information on the total coverage, whereas the latter measures the "in-plane" coverage, which accounts only the Bi adatoms in the (2×2) ordered domains with large enough size. Both intensity transient curves, as shown

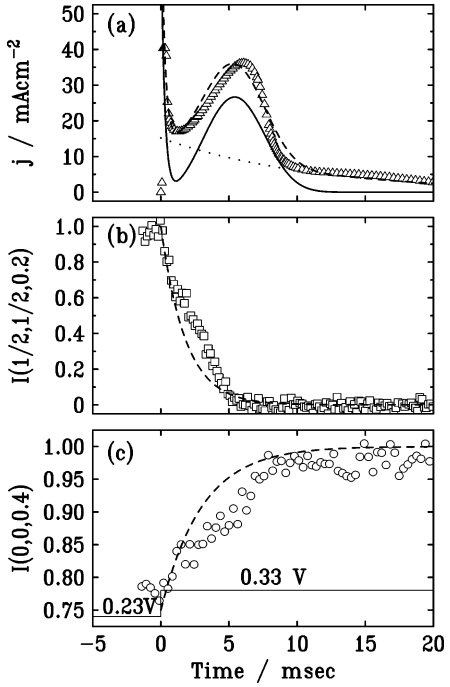

Figure 4. Current (a) and X-ray intensity transients (b) and (c) for the (2×2) → zero-coverage phase transition upon the potential step shown in (c). The dashed line in (a) shows the best fit to the data (triangles) by using eq 1, which is obtained with $n = 3$, $\tau_1 = 0.25$, $\tau_2 = 6.2$, $\tau_3 = 11$ ms, and $k_1 = 76$, $k_2 = 1.66$, $k_3 = 15.2$ mA/cm^2. The solid and dotted lines display the current components represented by the first two terms and the third term in eq 1, respectively. The dashed lines in (b) and (c) are generated by an exponential function to show the measured transients (squares and circles) exhibit nonexponential behavior.

in Figure 4b,c, deviate from a simple exponential function. At both positions, there is a rapid change in scattered intensity during the first 2 ms, a slower rate of change during the next 2 ms, and a second region of rapid change extending between 4 and 6 ms. These are consistent with the nonexponential behavior observed in the current transient, indicating the phase transition is a nucleation and growth type desorption.

The current transient, shown in Figure 4a, exhibits a well-defined peak at about 6 ms after the step change in the potential. This peak is reminiscent of the behavior expected for a nucleation and growth process, which can be described by the second term in the following equation,[3−5]

$$j = k_1 \exp(-t/\tau_1) + k_2 t^{n-1} \exp(-(t/\tau_2)^n) + k_3 \exp(-t/\tau_3) \quad (1)$$

where $k_{1,2,3}$ are the amplitudes and $\tau_{1,2,3}$ are time constants. The first and third terms are needed to account for the initial current spike that decays rapidly and the slopping background that extends beyond 12 ms, respectively. The integer, n, expresses the type of nucleation and growth process. With progressive growth, $n = 3$, the nucleation sites are constantly being created whereas for instantaneous growth, $n = 2$, all nucleation sites are created at the instant when the potential is stepped. The best fit was obtained with $n = 3$ and other parameters given in the figure caption.

It is noticed that the total charge from integration of the measured current transient is 313 μC/cm^2, which is significantly greater than the expected charge of 165 μC/cm^2 based on the transfer of 3 electrons per Bi atom, a Bi coverage change of a 0.25 monolayers, and an estimated area of 0.5 cm^2. Because

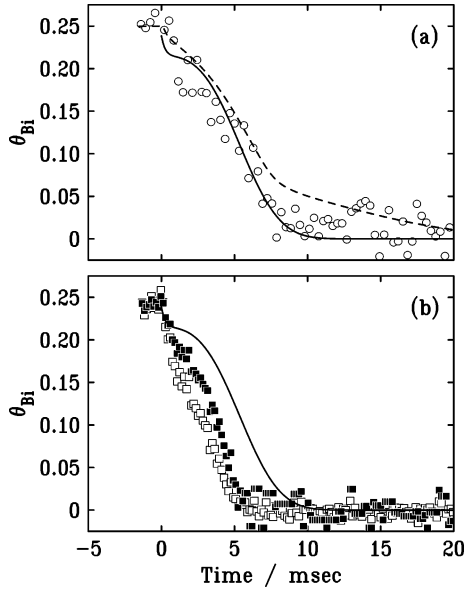

Figure 5. Bi coverage as a function of time deduced from the data shown in Figure 4. (a) Total coverage converted from the (0, 0, 0.4) intensity transient (circles) and from the charges by integrating the measured current (dashed line) and the current represented by the best fit with the slow exponential decay component subtracted (solid line). (b) "In-plane" coverage obtained from the intensity at the in-plane diffraction position, ($^1/_2$, $^1/_2$, 0.2), using the linear approximation (open squares) and the square root approximation (filled squares). The solid line in (a) is reproduced in (b) to facilitate the comparison between the "in-plane" coverage and the total coverage.

the X-ray intensity transients show the phase transition completes within 10 ms whereas the slow exponential decay extends over 20 ms, the slow exponential component (shown by the dotted line) is probably not directly related to the change of Bi coverage. This current appears to be caused by the so-called pseudocapacitance, often observed in electrodeposition of multivalent cations. It arises because an equilibrium is established between the intermediate Bi species, which can be partially discharged, and the Bi adatom. The potential change may cause a change in equilibrium and may not affect the total Bi coverage.[18] By excluding this component, the integrated charge (under the solid line) is reduced to 165 μC/cm^2.

Furthermore, the Bi coverage calculated from a linear relationship to the integrated charge is compared with that converted from the X-ray intensity transient at the (0, 0, 0.4) position. The open circles in Figure 5a show the time-dependent Bi coverage converted from the (0, 0, 0.4) intensity transient using the relationship, $\theta_{Bi} = 0.25 \times [1 - (I_{(0,0,0.4)} - 0.78)/0.22]$, which is an approximation of a simple kinematical model of the scattering intensity where the absorbed Bi interferes destructively with the underlying Au(111) substrate.[18] Within the context of this model, the relative intensity at (0, 0, 0.4) scales nearly linearly with Bi coverage between zero and 0.25 monolayer.[18] The dashed line shows the coverage, obtained from integration of the transient current shown in Figure 4a., which is in reasonable agreement with the coverage obtained from the specular reflectivity for small times but deviations are apparent at larger times. By excluding the current from the slow exponential decay in Figure 4a, the calculated coverage (solid line) is reduced at larger times. With this modification, the coverage is in better agreement with the coverage obtained from the specular reflectivity. The initial sharp change within the first millisecond cannot be attributed to the much faster 0.05 ms cell response associated with recharging the double layer.

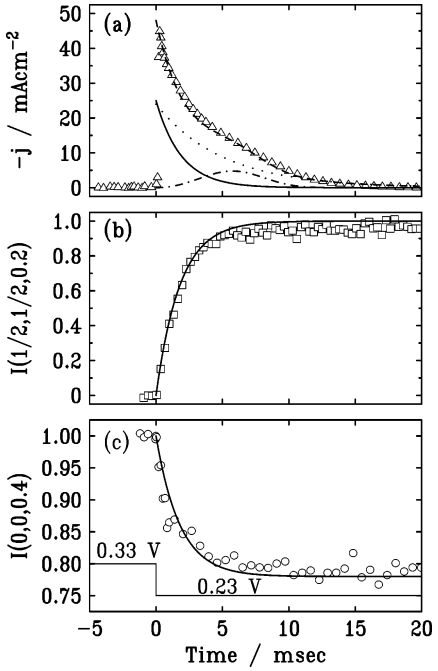

Figure 6. Current (a) and X-ray intensity transients (b) and (c) for the zero-coverage → (2×2) phase transition upon the potential step shown in (c). The dashed line in (a) shows the fit to the data (triangles) by using eq 1 with $n = 3$, $\tau_1 = 1.9$, $\tau_2 = 6.6$, $\tau_3 = 5.0$ ms, and $k_1 = 25$, $k_2 = 0.29$, $k_3 = 23$ mA/cm^2. Current components represented by the first, second, and third terms in eq 1 are shown by the solid, dash−dot, and dotted lines, respectively. In (b) and (c), the solid lines are the best fits to the data (squares and circles) by using eq 2, with $\tau =$ 1.8 ms for both cases.

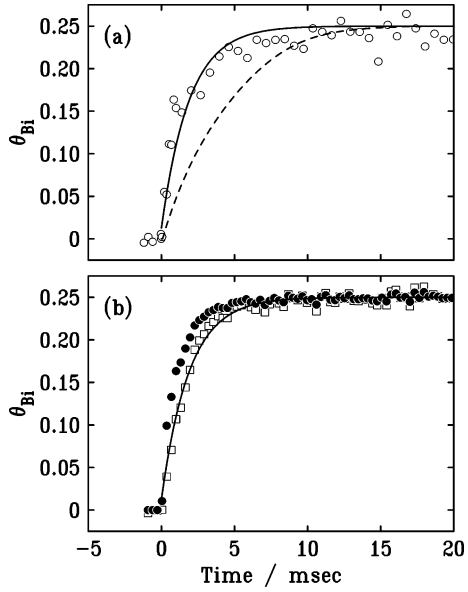

Figure 7. Bi coverage as a function of time deduced from the data shown in Figure 6. (a) Total coverage converted from the (0, 0, 0.4) intensity transient (circles), and from the charges by integrating the measured current (dashed line) and the current represented by the first fast exponential term (solid line). (b) "In-plane" coverage obtained from the intensity at the in-plane diffraction position, ($^1/_2$, $^1/_2$, 0.2), using the linear approximation (open squares) and the square root approximation (filled circles). The solid line in (a) is reproduced in (b) to facilitate the comparison between the "in-plane" coverage and the total coverage.

In Figure 5b the Bi coverage in the (2×2) superstructure is compared with the total coverage. Here the intensity at ($^1/_2$, $^1/_2$, 0.2) has been converted to an effective "in-plane" coverage assuming that the diffraction widths are independent of coverage. This is indeed the case when there is fast coarsening where the small, shrinking Bi domains would coalesce to form larger islands. These larger islands are likely to be resolution limited and in this case the peak intensity is a measure of the integrated intensity and both quantities depend linearly on the Bi coverage. However, the much faster decrease of the effective in-plane coverage compared to the other two measures of the coverage suggests that the peak intensity is not a good measure of the integrated intensity. For instance, small Bi islands, which shrink during the desorption process would give rise to a difference between the peak and integrated intensities. The corresponding line-shape broadening associated with these shrinking islands is very difficult to observe due to the high background originating from the electrolyte diffuse scattering signal. The formation of antiphase domains (shifts by half an overlayer lattice constant of the (2×2) Bi monolayer) is similar to coarsening in reverse, and this phenomenon would also give rise to line shape broadening. These antiphase domain defects are expected to appear at potentials where the attractive lateral interactions no longer favor a stable ordered (2×2) phase, as is the case after the potential is stepped positively. Regardless, our data clearly indicate that the desorption-induced loss of the (2×2) phase can be well described by a classic nucleation and growth process.

3.2.2. Zero-Coverage → (2 × 2)-Bi Phase Transition. In Figure 6 we show the results of current transient and X-ray scattering measurements for the zero-coverage → (2×2)-Bi phase transition. The X-ray intensity transients were measured at the same reciprocal space positions, ($^1/_2$, $^1/_2$, 0.2) and (0, 0, 0.4), as for the reverse transition discussed in the previous subsection. Both profiles, shown in Figure 6b,c, can be well described by an exponential form.

$$I(t) = k_0 + k_1 \exp(-t/\tau) \qquad (2)$$

where $I(t)$ is the normalized X-ray intensity at the peak, τ is the time constant, k_0 is the background, and k_1 is the amplitude. The best fits, shown as solid lines in Figure 6b,c give the same time constant of 1.8 ms. Because the Bi coverage scales linearly with the intensity at (0, 0, 0.4), albeit with a negative slope, the total Bi coverage, calculated from the intensity transient at (0, 0, 0.4) shown in Figure 7, increases in an exponential manner with time. This exponential behavior is consistent with a Langmuir type adsorption model where the adsorption is uniform across the entire surface.

The current transient, shown in Figure 6a, exhibits a near exponential behavior, which can be fitted to eq 1 with $n = 3$. Other parameters are given in the figure caption. The solid line shows the component represented by the first exponential term in eq 1, which has a time constant 1.9 ms, close to that measured by X-ray intensity transients (1.8 ms). The components represented by the second and third terms are also shown by the dot−dash and dotted lines, respectively. In Figure 7a, the total coverage obtained by converting the measured current (dashed line) and the current component represented by the fast exponential term (solid line) are compared to that obtained from the (0, 0, 0.4) intensity transient (circles). The good agreement of the solid line with the circles suggests that the other two current components are not directly related to the change of Bi coverage.

The integrated charge for the current components represented by the first, second, and the third terms are 49, 28, and 115 μC/cm^2, respectively. The sum of the charges for the two exponential components (the first and the third) is 164 μC/cm^2, nearly identical to the calculated value, which is also the charge

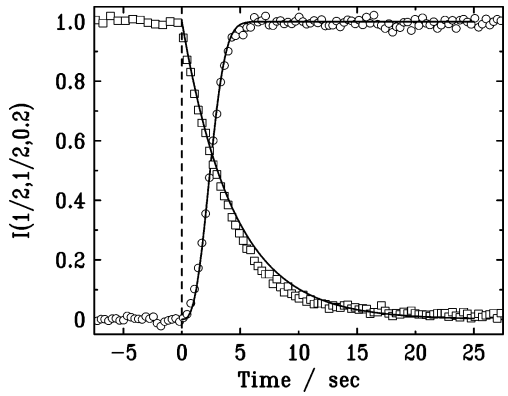

Figure 8. X-ray intensity transients measured at ($^1/_2$, $^1/_2$, 0.2) with potential steps from 0.17 to 0.27 V (circles) and from 0.27 to 0.17 V (squares). Solid lines are the best fits obtained by using eq 5 for the formation of the (2×2) phase (circles) with $\alpha = 1$ and $\tau = 1.7$ s, and by using a simple exponential function, eq 2, for the loss of the (2×2) phase with $\tau = 4.4$ s.

represented by the solid line in Figure 4a for the reversed phase transition. The excess charge represented by the second term may result from oxygen reduction due to a small, initial amount of dissolved oxygen exist in the solution drop.[18] This current rises first as the catalytic activity for oxygen reduction increases with the formation of the active (2×2)-Bi phase and eventually decreases due to the lack of a continuous oxygen supply.

How does the formation of an ordered phase follow the initial uniform adsorption? We consider three different scenarios. If the ordered phase only appears after a critical coverage is achieved, as is the case for Br adsorption on Ag(100), then the intensity at ($^1/_2$, $^1/_2$, 0.2) would lag behind the intensity at (0, 0, 0.4). Because both intensities show the same temporal behavior, we can rule out this scenario. For the case of slow lateral diffusion after the initial adsorption, coarsening occurs and the peak width at ($^1/_2$, $^1/_2$, 0.2) would sharpen with time. Under this scenario the intensity at ($^1/_2$, $^1/_2$, 0.2) would also lag behind the intensity at (0, 0, 0.4). The absence of a lag in the data also rules out the scenario. Further, we can also rule out the appearance of antiphase domains in the coarsening process because this would also broaden the peak and give rise to a discrepancy between the two intensities. The good agreement in the scattering intensities at both positions supports fast coarsening, on a time scale faster than 1 ms.

3.2.3. (2 × 2)-Bi ↔ (p × √3)-2Bi Phase Transition. The transition to the (p×√3)-2Bi phase from the (2×2)-Bi phase corresponds to an increase in the Bi coverage from 0.25 to 0.61. Whereas the low-coverage phase is commensurate, the higher coverage phase is uniaxially incommensurate. In Figure 8 we show the time dependent X-ray scattering intensity at ($^1/_2$, $^1/_2$, 0.2) after a potential step from 0.17 to 0.27 V (circles) and vice versa (squares). The potentials were chosen to have an equal and small overpotential for both directions, as discussed in section 3.1, and the duration at each potential was 40 s. Note that the time scale in the Figure 8 is seconds. Therefore, the transition is about a factor of 1000 slower than the transitions reported in the previous two sections. A slower phase transition is also suggested by the broader current peaks in the voltammetry compared to those at high potentials. The corresponding current transient is very slow and difficult to measure due to the small current, thus the X-ray measurements provide our only measure of the kinetics of this transition. Further, because the specular intensity at (0, 0, 0.4) does not depend strongly on the coverage in the range between 0.25 and 0.61,[18] it was not possible to provide a complementary measure of the coverage from this measurement. With only a single measure of the coverage, it is not possible to arrive at an unambiguous measure of the transition kinetics. However, on the basis of the functional form of the intensity dependence at ($^1/_2$, $^1/_2$, 0.2) we speculate that the adsorption appears Langmuir like whereas the opposite transition appears to follow nucleation and growth behavior. In the following analysis we have made the assumption that the domains are resolution limited.

For the (2×2) to (p×√3)-2Bi phase transition, the transient data shown by the squares in Figure 8 can be reasonably well described by an exponential decay with a time constant of 4.4 s, suggesting a Langmuir adsorption process. For the reversed phase transition, the data (circles) exhibit nonexponential behavior. According to the Avrami theorem, a general expression for nucleation and growth is given by

$$\theta = 1 - \exp(-\theta_{ext}) \tag{3}$$

where θ_{ext} is the extended coverage, which can be written as

$$\theta_{ext} = \alpha[(t/\tau)^2 - 2t/\tau + 2 - 2\exp(-t/\tau)] \tag{4}$$

The prefactor, $\alpha = \pi N_\infty (k_g/k_N\rho)^2$, depends on both the rate of nucleation k_N and the rate of growth, k_g, whereas the time constant, τ, equals to $1/k_N$.[28] The time dependence of the ($^1/_2$, $^1/_2$, 0.2) intensity can be described by combining eqs 3 and 4,

$$I = 1 - \exp\{-\alpha[(t/\tau)^2 - 2t/\tau + 2 - 2\exp(-t/\tau)]\} \tag{5}$$

The parameters, α and τ, are strongly correlated in the fits and we have fixed $\alpha = 1$, which gives $\tau = 1.7$ s for the best fit, as shown by the solid line in Figure 8. Our results suggest that the transition from the (2×2) Bi to (p×√3)-Bi phase transition is Langmuir-like whereas the reverse transition follows a nucleation and growth model.

4. Summary and Conclusions

The kinetics of Bi monolayer electrodeposition and the associated phase transitions on the Au(111) electrode has been measured using surface X-ray diffraction and electrochemical methods. The high energy, 32 keV X-rays utilized for this study allowed the use of a transmission cell, which provided a cell response time in the submillisecond range. Three independent measures of the Bi coverage transients were obtained, which are related to (1) the integrated charge, (2) the adsorbed Bi, irrespective of the adsorption site, and (3) the adsorbed Bi with a well-defined (2×2) structure. The zero-coverage ↔ commensurate (2×2)-Bi phase transition occurs on the millisecond time scale, 3 orders of magnitude faster than the (2×2)-Bi ↔ high-coverage incommensurate (p×√3)-2Bi phase transition. Classical nucleation and growth kinetics were observed for the (2×2)-Bi desorption transition in both the electrochemical and X-ray measurements. Further, the different time constants for the two different X-ray determined coverages suggests slow (relative to the nucleation time) coarsening behavior, as expected for the case of nucleation and growth kinetics. However, changes in the X-ray profiles, expected for the coarsening process were beyond our resolving limit; a consequence of the strong electrolyte background scattering. For the reverse transition, corresponding to the adsorption of Bi to form the (2×2) phase, Langmuir-like adsorption kinetics was observed. In this case, the X-ray and electrochemical measurements exhibit classical exponential profiles. The close agreement between the two X-ray measures of coverage suggests fast coarsening, on the submillisecond time scale, which is faster than the nucleation time.

These results suggest that the surface diffusion, which is what determines the rate of the coarsening process, is very different for the adsorption and desorption processes. Measurements were also carried out for the $(p\times\sqrt{3})$-2Bi to (2×2)-Bi phase transition, a transition that occurs on the second time scale. The intensity at (0, 0, 0.4) cannot be readily related to the coverage and without two independent measures of the coverage it is difficult to ascertain the coarsening. On the basis of the functional form of the intensity dependence at ($^1/_2$, $^1/_2$, 0.2), we speculate that the adsorption appears Langmuir-like whereas the opposite transition appears to follows nucleation and growth behavior. Despite the absence of observable changes in the scattering profiles, expected for coarsening phenomena, this study shows that combined electrochemical and X-ray scattering transients, at different reciprocal space positions, can provide detailed information on the nature of electrochemical transitions on the millisecond time scale.

Acknowledgment. We acknowledge fruitful discussions with Thomas Wandlowski, Stephen Feldberg, and Ian Robinson. This work is supported by the U.S. Department of Energy, Divisions of Chemical and Materials Science, under the contract no. DE-AC0298CH10886. K. Tamura acknowledges the Japan Society for the Promotion of Science for fellowships to do research abroad during the year 2000-2002.

References and Notes

(1) *Interfacial Electrochemistry*; Wieckowski, A., Ed.; Marcel Dekker: New York, 1999.

(2) Budevski, E.; Staikov, G.; Lorentz, W. J. *Electrochemical Phase Formation and Growth*; VCH Publishers: New York, 1996.

(3) Bewick, A.; Fleischmanm, M.; Thirsk, H. R. *Trans. Faraday Soc.* **1962**, *58*, 2200.

(4) Holzle, M. H.; Retter, U.; Kolb, D. M. *J. Electroanal. Chem.* **1994**, *371*, 101.

(5) Holzle, M. H.; Zwing, V.; Kolb, D. M. *Electrochim. Acta* **1995**, *40*, 1237.

(6) Xia, X. H.; Nagle, L.; Magnussen, O. M.; Behm, R. J. *Phys. Chem. Chem. Phys.* **2000**, 4387.

(7) Edens, G. J.; Gao, X.; Weaver, M. J. *Surf. Sci.* **1994**, *302*, L275.

(8) Gao, X.; Edens, G. J.; Hamelin, A.; Weaver, M. J. *Surf. Sci.* **1993**, *296*, 333.

(9) Gao, X.; Weaver, M. J. *J. Phys. Chem.* **1993**, *97*, 8685.

(10) Gao, X.; Edens, G. J.; Weaver, M. J. *J. Electroanal. Chem.* **1994**, *376*, 21.

(11) Naohara, H.; Ye, S.; Uosaki, K. *J. Electroanal. Chem.* **1999**, *473*, 2.

(12) Wano, H.; Uosaki, K. *Langmuir* **2001**, *17*, 8224.

(13) Finnefrock, A. C.; Buller, L. J.; Ringland, K. L.; Brock, J. D.; Abruna, H. D. *J. Am. Chem. Soc.* **1997**, *119*, 11703.

(14) Finnefrock, A. C.; Ringland, K. L.; Brock, J. D.; Buller, L. J.; Abruna, H. D. *Phys. Rev. Lett.* **1998**, *81*, 3459.

(15) DeVilbiss, J. E.; Wang, J. X.; Ocko, B. M.; Tamura, K.; Adzic, R. R.; Vartanyants, I. A.; Robinson, I. K. *Electrochim. Acta* **2002**, *47*, 3057.

(16) Wang, J.; Ocko, B. M. *Phys. Rev. B* **1992**, *46*, 10321.

(17) Samant, M. G.; Toney, M. F.; Borges, G. L.; Blum, L.; Melroy, O. R. *J. Phys. Chem.* **1988**, *92*, 220.

(18) Tamura, K.; Ocko, B. M.; Wang, J.; Adzic, R. R. *J. Phys. Chem. B* **2002**, *106*, 3896.

(19) Dickertmann, D.; Scultze, J. W. *Electrochim. Acta* **1977**, *22*, 117.

(20) Schultze, J. W.; Dickertmann, D. *Faraday Symp. Chem. Soc.* **1977**, *12*, 36.

(21) Schultze, J. W.; Dickertmann, D. *Ber. Bunsen-Ges. Phys. Chem.* **1978**, *82*, 528.

(22) Adzic, R. R.; Jovancicevic, V.; Podlavicky, M. *Electrochim. Acta* **1980**, 1143.

(23) Chen, C. H.; Gewirth, A. A. *J. Am. Chem. Soc.* **1992**, *114*, 5439.

(24) Chen, C. H.; Kepler, K. D.; Gewirth, A. A.; Ocko, B. M.; Wang, J. *J. Phys. Chem.* **1993**, *97*, 7290.

(25) Oh, I.; Biggin, M. E.; Gewirth, A. A. *Langmuir* **2000**, *16*, 1397.

(26) Niece, B. K.; Gewirth, A. A. *Langmuir* **1996**, *12*, 4909.

(27) Li, X.; Gewirth, A. A. *J. Am. Chem. Soc.* **2003**, *125*, 7086.

(28) Finnefrock, A. C. Time-resolved Measurements of the underpotential deposition of copper onto platinum(111) in the presence of chloride, Cornell University, 1998.